Title

NLR surveillance of essential SEC-9 SNARE proteins induces programmed cell death upon allorecognition in filamentous fungi

Journal

Proceedings of the National Academy of Sciences of the United States of America, 115(10)

ISSN

0027-8424

Authors

Heller, Jens

Clavé, Corinne

Gladieux, Pierre

et al.

Publication Date

2018-03-06

DOI

10.1073/pnas.1719705115

Peer reviewed

NLR surveillance of essential SEC-9 SNARE proteins induces programmed cell death upon allorecognition in filamentous fungi

Jens Heller[1,2], Corinne Clavé[3], Pierre Gladieux[4], Sven J. Saupe[3] and N. Louise Glass[1,2*]

[1]The Plant and Microbial Biology Department, The University of California, Berkeley, CA 94720-3102

[2]Environmental Genomics and Systems Biology Division, Lawrence Berkeley National Laboratory, 1 Cyclotron Road, Berkeley, CA 94720

[3]Institut de Biochimie et de Génétique Cellulaire, CNRS, Université de Bordeaux, 33077 Bordeaux, France

[4]BGPI, University of Montpellier, INRA, CIRAD, Montpellier SupAgro, F-34398 Montpellier, France

*Correspondence: Lglass@berkeley.edu

Short title:

Death induction by a fungal NOD-like receptor

Classification:

Biological Sciences, Genetics

Keywords

NOD-like receptors, allorecognition, trans-species polymorphism, balancing selection, SEC-9 SNARE, fungal immunity, Neurospora, Podospora

Abstract

In plants and metazoans, intracellular receptors that belong to the NOD-like receptor (NLR) family are major contributors to innate immunity. Filamentous fungal genomes contain large repertoires of genes encoding for proteins with similar architecture to plant and animal NLRs with mostly unknown function. Here, we identify and molecularly characterize PLP-1, an NLR-like protein containing an N-terminal patatin phospholipase domain, a nucleotide binding domain and a C-terminal tetratricopeptide repeat (TPR) domain. PLP-1 guards the essential SNARE protein SEC-9; genetic differences at *plp-1* and *sec-9* function to trigger allorecognition and cell death in two distantly related fungal species, *Neurospora crassa* and *Podospora anserina*. Analyses of *Neurospora* population samples revealed that *plp-1* and *sec-9* alleles are highly polymorphic, segregate into discrete haplotypes and show trans-species polymorphisms. Upon fusion between cells bearing incompatible *sec-9* and *plp-1* alleles, allorecognition and cell death are induced, and which is dependent upon physical interaction of SEC-9 and PLP-1. The central nucleotide binding domain and patatin phospholipase activity of PLP-1 are essential for allorecognition and cell death, while the TPR domain and the polymorphic SNARE domain of SEC-9 function in conferring allelic specificity. Our data indicates that fungal NLR-like proteins function similarly to NLR immune receptors in plants and animals, showing that NLRs are major contributors to innate immunity in plants and animals and for allorecognition in fungi.

Significance

NOD-like receptors are fundamental components of plant and animal innate immune systems. Some fungal proteins with NLR-like architecture are involved in an allorecognition process that results in cell death, termed heterokaryon incompatibility. A role for fungal NLR-like proteins in pathogen defense has also been proposed. Here, we show that a fungal NLR-like protein, PLP-1, monitors the essential SNARE protein SEC-9 in two distantly related fungal species, *Neurospora crassa* and *Podospora anserina*. Both *plp-1* and *sec-9* are highly polymorphic in fungal populations and show evidence of balancing selection. This study provides biochemical evidence that fungal NLRs function

similarly to NLRs in plants and animals, indicating that these fundamental players of innate immunity evolved independently in all three kingdoms.

\body

Introduction

STAND-like NTPases are broadly distributed across all domains of life, potentially facilitated by horizontal gene transfer (1). In plants and metazoans, intracellular STAND-like NTPases of the nucleotide-binding domain (NBD), leucine-rich repeat (LRR) superfamily serve as sensors of pathogen derived effector proteins (plants and metazoans) and pathogen associated molecular patterns (metazoans), making them major constituents of innate immunity (2, 3). Upon pathogen recognition, these NOD-like receptors (NLRs) control programmed cell death (PCD) reactions in plants (hypersensitive response) and metazoans (apoptosis, pyroptosis, necroptosis) to prevent the spread of the infection (3-5).

NLR proteins have a characteristic tripartite domain organization with a central NBD, an N-terminal downstream-acting domain and C-terminal ligand-binding domains composed of superstructure-forming repeats (3). Despite similar modes of action of plant and metazoan NLRs and the involvement of related domains, phylogenetic analyses suggest that the typical domain architecture evolved *de novo* and independently (6). The genomes of filamentous fungi also encode genes with a core architecture similar to animal and plant NLRs. Some characterized fungal NLRs have been associated with a conspecific allorecognition process termed heterokaryon incompatibility (HI) (7, 8). During HI, heterokaryotic cells that are generated via cell fusion between genetically incompatible strains are rapidly compartmentalized and undergo PCD (7). HI has been shown to restrict mycovirus transfer between fungal colonies (9). Because an additional role for fungal NLR-like proteins during xenorecognition as part of a fungal innate immune system has been proposed (10, 11), an understanding of fungal NLR function could serve as a basis to study the general evolutionary origin of NLR-mediated pathogen defense and innate immunity.

Molecular models of NLR proteins are mostly based on studies in plants and metazoans. Intra-molecular domain interactions are thought to keep NLRs in

a suppressed state. Recognition of xenogeneous ligands (*e.g.* PAMPS or pathogen effectors (12)), but also allogeneous ligands (*e.g.* during hybrid necrosis (13)) via C-terminal LRRs induces conformational changes that activate the NBD, thus initiating downstream reactions via functions of the N-terminal domains (14). Oligomerization can be part of the activation of animal NLRs (15). Several plant NLRs have been hypothesized to also form oligomers, although the function of the NBD for plant NLR oligomerization remains unresolved (16). The conserved domain architecture of NLRs across kingdoms suggests that similar modes of activation occur even if primary sequences and downstream functions can be diverse.

Here, we molecularly characterize a filamentous fungal NLR controlling an allorecognition and PCD process that acts at the germling stage (*i.e.* in germinated asexual spores), a process termed germling regulated death (GRD). In a *Neurospora crassa* population, the GRD phenotype was associated with polymorphisms at the *sec-9* and *plp-1* loci. Cells from different GRD haplotypes (and thus with alternative alleles at *sec-9* and *plp-1*) underwent rapid cell death following germling fusion. The *sec-9* locus encodes an essential SNARE (Soluble NSF Attachment Protein Receptor) protein, while *plp-1* encodes a fungal NLR. Co-immunoprecipitation experiments showed that interactions of incompatible SEC-9 and PLP-1 encoded by different haplogroups induce PLP-1 oligomerization associated with PCD. Additionally, we show that orthologs of *sec-9* and *plp*-1 in *Podospora anserina,* which diverged from *N. crassa* ~75 mya, also mediate allorecognition and PCD. These data indicate the importance of this NLR-based surveillance system of the SEC-9 SNARE in filamentous fungi and show that common molecular mechanism underlies NLR function in animals, plants and fungi.

Results

GRD haplotypes in a *N. crassa* population are associated with genomic rearrangements and with loci that encode highly divergent alleles.

Analysis of germling communication phenotypes between wild isolates of a *N. crassa* population (17) revealed that some fused germling pairs between genetically different wild isolates die ~20 min post-fusion, indicated by strong

vacuolization, cessation of cytoplasmic flow and uptake of the vital dye SYTOX® Blue (S1 Movie, S2 Movie). We refer to this rapid cell death phenotype following fusion as germling regulated death (GRD) (Fig. 1).

Death rates of fused germlings were quantified using vital dyes and flow cytometry (see Material and Methods; Fig. S1A, B). Germlings from single strains (self fusion) showed death frequencies of ~5%. When germlings of different GRD background were paired, death frequencies significantly increased (~50%) (when mixed in a 1:1 ratio, ~50% germling death rate corresponds to the maximal death rate to be expected if all fused germlings of different GRD background die). Importantly, GRD was not germling specific, but also occurred after fusion of mature hypha of different GRD background. Analyses of the segregation of the GRD phenotype in F1 progeny from a cross between a GRD1 strain (FGSC 2489) and a GRD3 strain (JW258) showed that the GRD phenotype segregated as a Mendelian trait.

To identify the GRD locus, we performed a bulk segregant analysis and whole genome re-sequencing of progeny pools with identical GRD phenotype from a backcross of F1 progeny with a GRD1 strain (FGSC 2489). Bulked segregant analysis revealed a ~180 kbp region on the right arm of linkage group I (LGI) that showed segregation of SNPs between the different GRD phenotype pools at ~100% frequency (Fig. S2A). A random SNP distribution was observed for the rest of LGI and for the remaining 6 LGs of *N. crassa*.

To further refine the GRD locus within the ~180 kbp region, re-sequencing data from 23 wild isolates from this same *N. crassa* population was analyzed (18), revealing a 55 kbp region that showed four different genomic rearrangements spanning 21 loci (NCU09237 to NCU09253; gene nomenclature based on the reference genome FGSC 2489 (19)). We refer to these genomic rearrangements as germling regulated death haplotype 1 through 4 (GRDH1-4) (Fig. 2A). To determine whether structural differences between GRDHs were associated with nucleotide differences in particular genes, we used sequence alignments to characterize the nature and level of variability of genes within and between the haplogroups. Among the loci in the genetic interval associated with GRDHs, only NCU09243 and NCU09244 displayed high levels of allelic variability in the genomes of the 23 isolates (Table S1; Fig. S2B). Both genes were among

the most polymorphic genes of the *N. crassa* population, in the top 0.1% for the number of polymorphic sites S and nucleotide diversity π (comparison with a set of 8621 reference genes from (18)). High positive Tajima's D values indicated the presence of NCU09243 and NCU09244 alleles at an intermediate frequency in the population, and gene genealogies revealed four long-diverged haplogroups (Table S2; Fig. 2A, B; Fig. S2C, E) that correlated with the genomic rearrangements of the four GRDHs. Alleles at NCU09243 and NCU09244 between members of different GRDHs were highly divergent with nucleotide divergence per site ranging from 25% to 49%. In contrast, nucleotide diversity of NCU09243 and NCU09244 alleles within a single GRDH was 2 orders of magnitude lower than divergence between GRDHs (π ranging from 0 to 0.01105/bp), comparable with the rest of the genome (average π=0.007416/bp; sd: 0.008449). All other genes in the 55 kbp region were significantly less polymorphic than NCU09243 and NCU09244 (Fig. S2B, C) and gene genealogies did not show long-diverged haplotypes (Fig. 2A, B; Fig. S2D). Exceptions were NCU09247 and NCU16494, which showed high Tajima's D values (D=1.40, D=1.42, respectively), but haplotype groups in these genes did not track with GRDHs (Fig. S2C, D). The GRDH2, GRDH3 and GRDH4 strains also contain a duplication of NCU09244, but are missing NCU09245, which is only present in GRDH1 strains (Fig. 2A). Both NCU09244 and NCU09245 encode proteins with predicted patatin-like phospholipase domains suggesting they are paralogs, in spite of low total amino acid sequence identity (~18%) (Table S1). In addition to the N-terminal patatin phospholipase domain, NCU09244 also has a nucleotide binding domain (NB-ARC type) and C-terminal tetratricopeptide repeats (TPR), a domain structure described for NOD-like receptors (3, 10). We called this gene *plp-1* (patatin-like phospholipase). NCU09245 has a similar structure to PLP-1 but is missing the NBD domain. NCU09245 was named *plp-2*.

NCU09243 has homology to the t-SNARE protein Sec9 of *Saccharomyces cerevisiae*, which is required for secretory vesicle-plasma membrane fusion (20). We therefore named NCU09243 *sec-9*. The *plp-1* and *sec-9* genes of *N. crassa* are orthologs of *vic-2* and *vic-2a,* respectively, that confer *vic-2* vegetative incompatibility in the chestnut blight fungus *Cryphonectria parasitica* (21).

Alleles at *sec-9* and *plp-1/plp-2* show signatures of balancing selection.

The finding of four highly divergent GRD haplotypes suggested a relatively ancient origin of the GRD locus. To test this hypothesis, we performed phylogenetic analyses of alleles at NCU09242 through NCU09247 from the 23 wild *N. crassa* isolates, as well as alleles at these same loci from a population sample from the distantly related species *Neurospora discreta*. For NCU09242, NCU16494, and NCU09247 allelic lines from within species were reciprocally monophyletic (Fig. 2B; Fig. S2D), as predicted by theory (22), given the estimated divergence time between *N. crassa* and *N. discreta* (7–10 million years ago (23)) and their effective population size (circa 10^6 and 10^4 individuals, respectively (24, 25)). However, for *sec-9* and *plp-1*, no reciprocal monophyly was observed, indicating that the age of allelic lines exceeds the age of speciation events (Fig. 2B; Fig. S2E). This phenomenon is referred to as trans-species polymorphism (TSP) and has been observed in *N. crassa* for other loci involved in non-self recognition (17, 18, 26). The observed pattern of TSP is consistent with balancing selection and limited recombination among alleles causing the evolution of highly divergent haplogroups. Inferred genealogical histories of *sec-9*, *plp-1*, and *plp-2* were in fact concordant with differences in patterns of genomic arrangements among GRD haplotypes, suggesting limited recombination across the whole region: alleles from GRDH1 to GRDH4 were in distinct clades for *sec-9*, *plp-1*/*plp-2* (*plp-2* was in a separate clade, because it is only present in GRDH1 strains, while *plp-1.2* of GRDH3 and GRDH4 sequences clustered together (Fig. 2B; Fig. S2E).

Non-allelic genetic interactions between *plp-1* and *sec-9* mediate GRD

Based on the evolutionary analyses of genes within the GRDHs, we hypothesized that genetic interactions between *sec-9* and/or *plp-1*/*plp-2* confer GRD. To test this hypothesis, we first examined strains carrying single deletions of *plp-1* or *plp-2* and strains bearing deletions of both *plp-1* and *plp-2* in a GRD1 background. The *Δplp-1*, *Δplp-2* and *Δplp-1 Δplp-2* strains were macroscopically indistinguishable from their parental strain and displayed similar death frequencies in self pairings (Fig. S1C). In allogenic (nonself) pairings, all three mutants (*Δplp-1*, *Δplp-2* and *Δplp-1 Δplp-2*) displayed the GRD specificity of their

isogenic GRD1 parent; *i.e.* ~50% germling death frequency when paired with a GRD3 strain (Fig. 3A). These data indicated that GRD is not mediated by allelic interactions between *plp-1* or *plp-2* alleles, or by non-allelic *plp-1/plp-2* interactions.

Attempts to construct a *sec-9* deletion strain were unsuccessful, indicating *sec-9* is an essential gene in *N. crassa*, similar to *S. cerevisiae SEC9* (27). Therefore, we created swap strains where the *sec-9*^{GRD1} allele in a *Δplp-1 Δplp-2* strain (GRD1 background) was replaced with *sec-9* alleles from other haplogroups (GRDH2, GRDH3 or GRDH4) (Fig. 3B). All of these *sec-9* swap strains showed increased germling death frequencies when paired with the parental GRD1 strain (20-40%) (Fig. 3C). These data indicated that either allelic interactions between *sec-9* or non-allelic interactions between *sec-9* and *plp-1* and/or *plp-2* were required to induce GRD. To distinguish these possibilities, we paired germlings containing alternate *sec-9* alleles, but which both lacked *plp-1* and *plp-2*; death frequencies in these pairings were similar to self-death frequencies (Fig. 3C; Fig. S1C), indicating that allelic differences at *sec-9* were not sufficient to induce allorecognition and germling death. To test if non-allelic interactions between *sec-9* and *plp-1* and/or *plp-2* are important for GRD, germling death frequencies were assessed when *sec-9* swap strains (*sec-9*^{GRD2} or *sec-9*^{GRD3} or *sec-9*^{GRD4}, all in a *Δplp-1 Δplp-2* background) were paired with *sec-9*^{GRD1} strains bearing either *Δplp-1* or *Δplp-2* deletions. Significantly, cell death rates were reduced in pairings with the *sec-9*^{GRD1} *Δplp-1* strain, but not in pairings with the *sec-9*^{GRD1} *Δplp-2* strain (Fig. 3C). These data indicated that non-allelic interactions between *sec-9* and *plp-1* mediate allorecognition and GRD.

The *sec-9/plp-1* non-allelic interactions among the different haplogroups were confirmed to be essential for GRD by analyzing cell death in pairings of a GRD3 strain with all *sec-9* swap strains. As expected, pairings between the GRD3 and *sec-9*^{GRD3} *Δplp-1 Δplp-2* germlings showed low death frequencies (~5%). In contrast, pairings between the GRD3 strain and the *sec-9*^{GRD1} *Δplp-1 Δplp-2* strain showed high death frequencies (~50%), as did pairings between the GRD3 strain and the *sec-9*^{GRD2} *Δplp-1 Δplp-2* strain. However, pairings between the GRD3 strain and the *sec-9*^{GRD4} *Δplp-1 Δplp-2* strain showed intermediate death

frequencies (~15%) (Fig. S3A). Notably, the phylogeny of *sec-9/plp-1* showed that GRDH3 is more similar to GRDH4 than to GRDH1 or GRDH2 (Table S1).

Not all non-allelic *sec-9*/*plp-1* interactions induced GRD (Fig. S3B–E). For example, an engineered strain carrying the duplicated *plp-1* gene (*Δplp-1 Δplp-2, sec-9^{GRD2} plp-1.1^{GRD2}*) showed low death frequencies when paired with all *sec-9* swap strains (*i.e.* non-allelic interaction of *plp-1.1^{GRD2}* and *sec-9* does not mediate GRD) (Fig. S3C). However, pairings of a *sec-9^{GRD2}* strain carrying the second *plp-1* gene (*Δplp-1 Δplp-2, sec-9^{GRD2} plp-1.2^{GRD2}*) showed high death frequency when paired with *sec-9^{GRD3} Δplp-1 Δplp-2* or *sec-9^{GRD4} Δplp-1 Δplp-2* germlings, but showed low death frequency in pairings with *sec-9^{GRD1} Δplp-1 Δplp-2* (*i.e*. non-allelic interactions of *plp-1.2^{GRD2}* with *sec-9^{GRD3} and sec-9^{GRD4}* mediates GRD) (Fig. S3C). These data show that several specific non-allelic *sec-9*/*plp-1* interactions induce GRD while other non-allelic *sec-9/plp-1* interactions have no effect. However, because one incompatible *sec-9/plp-1* pair is sufficient to induce GRD, no viable heterokaryons will form between wild isolates of different GRDH. A potential increase of death frequencies in the presence of several paralogous *plp-1* genes cannot be excluded.

SNARE domains of SEC-9 mediate allelic specificity

SNARE proteins like SEC-9 are involved in fusion of vesicles with their target membranes; the SNARE domains are essential for formation of the coiled-coil structure with interaction partners Sso1p and Snc1p (28). Consistent with its potential function as a SNARE protein, GFP-tagged SEC-9 localized as a crescent at the germling tip (Fig. 2C; Fig. S2F). The N-terminus of SEC-9 (first 174 aa) was fairly conserved within the different GRD specificity groups and contained only a few amino acid substitutions that track with GRD haplotype. In contrast, the C-terminal region of SEC-9, which includes the SNARE domains essential for protein function, was highly diverse between the different GRD groups (Fig. 4A, B). A sliding window analysis of divergence between *sec-9* sequences from distinct haplogroups confirmed that divergence was higher around the coiled-coil domains (aa positions ~200-300) (Fig. S3F). To delineate the region of SEC-9 that confers allelic specificity, SEC-9 chimeras were constructed that consisted of the N-terminus of SEC-9 from a GRD3 strain fused

to the C-terminus of SEC-9 from a GRD1 strain or vice versa; chimeras replaced the *sec-9*^{GRD1} allele in a *Δplp-1 Δplp*-2 strain (Fig. 3B). A strain expressing the SEC-9 chimera with the GRD3 N-terminus and a GRD1 C-terminus showed high death frequencies (~45%) when paired with a GRD3 strain. A strain expressing a SEC-9 chimera with the GRD3 C-terminus showed high death frequencies (~35%) when paired with a GRD1 strain (Fig. 4C). These data indicated that the C-terminus, which includes the SNARE domains of SEC-9, mediates GRD allelic specificity.

To determine whether the SNARE domains alone were sufficient for recognition, we expressed isolated SNARE domains of SEC-9^{GRD3} (SNARE1: aa 191 to aa 257 or SNARE2: aa 360 to aa 422) in a *sec-9*^{GRD1} *Δplp-1 Δplp*-2 strain. We then assessed cell death frequencies when these strains were paired with a GRD1 strain (Fig. 4D). The vacuolization phenotype of GRD in fused germlings was assessed, as other GRD related phenotypes were weaker than with full length SEC-9. Vacuolization rates were low (~3%) in self-pairings between *sec-9*^{GRD1} *Δplp-1 Δplp-2* (*SNARE1*$^{sec\text{-}9\ GRD3}$) or between *sec-9*^{GRD1} *Δplp-1 Δplp-2* (*SNARE2*$^{sec\text{-}9\ GRD3}$) germlings (absence of PLP-1) (Fig. 4D). However, in pairings between *sec-9*^{GRD1} *Δplp-1 Δplp*-2 (*SNARE1*$^{sec\text{-}9\ GRD3}$) or *sec-9*^{GRD1} *Δplp-1 Δplp*-2 (*SNARE2*$^{sec\text{-}9\ GRD3}$) and a GRD1 strain (PLP-1 present), high vacuolization rates were observed in fused germling pairs (~30%) (Fig. 4D). These data indicated that either of the highly polymorphic SNARE1 and SNARE2 domains of SEC-9 mediate allelic specificity and were sufficient to induce GRD.

In *S. cerevisiae*, Sec9p physically interacts with syntaxin (Sso1/2p) and synaptobrevin (Snc1/2p) (28). Surprisingly, unlike *sec-9*, no polymorphisms that result in GRDH specific amino acid substitutions were present in *sso-1* (NCU02460) or *snc-2* (NCU00566) alleles in the *N. crassa* population (Table S1). Thus, SEC-9 proteins from the four different haplogroups function with identical SSO-1 and SNC-2 proteins for SNARE assembly and vesicle trafficking, a hypothesis supported by the fact that the *sec-9* swap mutants were viable.

To assess the correlation of diverse SEC-9 protein interactions with conserved SSO-1 and SNC-1 homologs, the level of amino-acid polymorphism and divergence at SNARE domains of SEC-9 across three fungal species (*N. crassa*, *P. anserina* and *C. parasitica*) was determined. Amino-acid variants were

mapped onto a predicted structure of the SNARE domains obtained by homology modeling onto Sec9p. Nearly the entire exposed surface of the SNARE domains showed extreme levels of variation. A reduced level of variation was only detected in a few positions predicted to form the interface with SSO-1 and SNC-1 homologs (Fig. 4E, F). This conservation of essential amino acids in SEC-9 that are associated with interactions with SSO-1 and SNC-1 homologs is consistent with the conserved essential function of SEC-9 despite general sequence diversity in filamentous fungal species.

PLP-1 is a fungal NOD-like receptor

The data presented above shows that GRD is a regulated process that depends on non-allelic interactions between *sec-9* and *plp-1*. PLP-1 has a tripartite domain architecture of an NLR (Fig. 5A). In contrast, PLP-2 is missing an NBD. Cellular localization studies using functional C-terminal tagged proteins (GFP and mCherry) showed that both PLP-1 and PLP-2 localize to the periphery of the cell (Fig. 2C; Fig. S2G). Protein and nucleotide alignments of PLP-1 from the 23 sequenced wild isolates indicated that the patatin-like domain and the NBD domain showed some conserved motifs, both within and between GRDHs (Fig. S3G-I). Sequence divergence was more heterogeneous and diversity was higher along the TPR helical domain (Fig. S3H, I).

Patatin-like domains have a conserved GGxR/K motif and a catalytic dyad formed by a serine and aspartic acid residue (29). The GGxR/K motif is conserved in PLP-1 and the predicted catalytic dyad is formed by serine 64 and aspartic acid 204 (Fig. 5B). In the NBD domain of PLP-1, the Walker A motif (GxxGxGKS/T), which is required for nucleotide binding, and the Walker B motif (xLhhhD), which is required for nucleotide hydrolysis, are conserved (Fig. 5C).

To test the hypothesis that the phospholipase catalytic activity and NBD motifs identified in PLP-1 are essential for GRD function, we generated four point mutations affecting either of the two residues of the catalytic dyad of the patatin-like domain (S64A or D204A) and the P-loop motif (Walker A; K414A), or the Walker B motif (D484A) of the NBD domain (Fig. 5B, C). These constructs were introduced into the *sec-9*^{GRD1} *Δplp-1 Δplp-2* strain. The mutated proteins retained their native localization to the periphery of the cell (Fig. 5D). However, the

activity of these proteins in mediating GRD was strongly affected (Fig. 5E). The *sec-9^{GRD1} Δplp-1 Δplp-2* strain expressing GFP-tagged wild type PLP-1 showed high death rates (~30%) when paired with a *sec-9^{GRD3} Δplp-1 Δplp-2* strain, but the *sec-9^{GRD1} Δplp-1 Δplp-2* strains expressing PLP-1^{S64A}, PLP-1^{D204A}, or PLP-1^{K414A} mutations showed low death rates (~5%). The *sec-9^{GRD1} Δplp-1 Δplp-2* strains expressing PLP-1^{D484A} (Walker B motif mutation) still induced some death (~15%) when paired with a *sec-9^{GRD3} Δplp-1 Δplp-2* strain. These data indicated that PLP-1 requires functional patatin phospholipase activity and a functional nucleotide-binding domain for full GRD function.

Physical interaction of incompatible SEC-9 and PLP-1 induces PLP-1/PLP-2 complex formation

Studies of NLRs in other organisms have suggested a model where ligand recognition results in a conformational change that relieves autoinhibitory intramolecular interactions, allowing NOD domain-dependent nucleotide binding and oligomerization, which in turn activates downstream reactions (30). To examine if PLP-1 functions similarly to other NLRs, we performed co-immunoprecipitation (co-IP) experiments to test physical interactions between SEC-9, PLP-1 and/or PLP-2 by creating strains that expressed differentially tagged PLP-1, PLP-2 and SEC-9 proteins (GFP/mCherry). We first assessed self-assembly of PLP-1^{GRD1}, self-assembly of PLP-2^{GRD1} and interaction between PLP-1^{GRD1} and PLP-2^{GRD1} in the absence of GRD; no interaction was detected (Fig. 6A). To assess interactions between PLP-1^{GRD1} and PLP-2^{GRD1} after GRD induction, GRD1 germlings expressing the tagged proteins were paired with a GRD3 strain. Self-assembly of PLP-1^{GRD1} and interaction of PLP-1^{GRD1} with PLP-2^{GRD1} was detected (Fig. 6B; Fig. S4A). However, interactions between SEC-9^{GRD1} with either PLP-1^{GRD1} or PLP-2^{GRD1} were not detectable independently of GRD induction (Fig. 6C; Fig. S4B). These data indicated that physical interaction/oligomerization of PLP-1 and PLP-2 of identical GRD specificity occurred under conditions of GRD, but not between SEC-9 and PLP-1/PLP-2 of identical GRD specificity.

Since non-allelic genetic interactions between *sec-9* and *plp-1* induced GRD (Fig. 3), we hypothesized that molecular recognition occurs via a physical interaction when SEC-9 and PLP-1 are of different GRD specificity. To test this

hypothesis, we created GFP labeled SEC-9^{GRD3} constructs driven by the *tef-1* promoter (high constitutive expression) or driven by its native *sec-9* promoter. Co-IP experiments were performed on strains expressing GFP labeled SEC-9^{GRD3} paired with strains expressing mCherry labeled PLP-1^{GRD1} or PLP-2^{GRD1}. Importantly, PLP-1^{GRD1} and SEC-9^{GRD3} co-immunoprecipitated, while an interaction between PLP-2^{GRD1} with SEC-9^{GRD3} was not detectable (Fig. 6C; Fig. S4B). These data indicated that SEC-9 and PLP-1 of different GRD specificity physically interact during the GRD reaction while SEC-9 and PLP-2 do not.

While the patatin-like domain as well as the NB-ARC domain of PLP-1 is necessary for GRD (Fig. 5E), it was unclear if the oligomerization of PLP-1/PLP-2 proteins is necessary and sufficient for GRD. We reasoned that mutations introduced in these domains that prevented GRD may also abolish protein-protein interactions. To test this hypothesis, strains expressing mutated versions of GFP and mCherry labeled PLP-1 (mutations in the catalytic dyad of the patatin-like domain, S64A or D204A, or NBD mutations in the P-loop motif, K414A or the Walker B motif, D484A) were paired with a *sec-9*^{GRD3} *Δplp-1 Δplp-2* strain. Co-IP experiments showed that mutations in the NBD domain (K414A, D484A) prevented the self-association of PLP-1 proteins (Fig. 6D; Fig. S4C). In contrast, mutations in the patatin-like domain (S64A, D204A) did not affect self-association of PLP-1 (Fig. 6D; Fig. S4C), even though these mutations completely eliminated GRD (Fig. 5E). These data indicated that self-association of PLP-1 via the NB-ARC domain is not sufficient for GRD. Instead, a functional patatin-like domain is essential to transmit the GRD signal.

We reasoned that SEC-9^{GRD3} might interact with PLP-1^{GRD1} containing mutations in the NB-ARC domain or in the patatin-like domain, despite the lack of GRD. To test this hypothesis, we co-cultivated strains expressing mutated versions of mCherry labeled PLP-1^{GRD1} (S64A or K414A) with a *Δplp-1 Δplp-2* strain expressing SEC-9^{GRD3}–GFP. In co-IP experiments, a strong interaction between SEC-9^{GRD3} with PLP-1^{S64A} (catalytic dyad mutation) was observed, while a weak interaction between SEC-9^{GRD3} with PLP-1^{K414A} (Walker A motif mutation) was detected (Fig. 6C). These data support the hypothesis that recognition of SEC-9 by PLP-1 is not affected by mutations in the NBD or the patatin-like domains. A weak interaction of SEC-9^{GRD3} with PLP-1^{K414A} could be explained by

the lack of signal enhancement due to the lack of PLP-1^{K414A} self-association. Together, these data indicated that the interaction between SEC-9 and PLP-1 of different GRD specificity is independent of NBD function and patatin-like activity and occurs even in the absence of GRD.

sec-9 and *plp-1* homologs determine *het-z* heterokaryon incompatibility in *Podospora anserina*

In *C. parasitica*, orthologs of *plp-1* and *sec-9* are associated with heterokaryon incompatibility mediated by allelic differences at the *vic2* locus (21). In a systematic search of molecular components of *het* loci in other fungi, we determined that *sec-9/plp-1* orthologs mediate *het-z*-incompatibility in *P. anserina* (Fig. S5A). *Het-z* is one of nine heterokaryon incompatibility loci of *P. anserina,* with two allelic specificities, *het-z1* and *het-z2,* defining the incompatibility system. If strains of different *het-z* specificity fuse, they show characteristic cell death reactions and barrage formation at the contact point between incompatible colonies (Fig. S5A). *het-z* incompatibility was assessed via transformation efficiency tests; *i.e.* transformation efficiency was reduced when *PaSec9$^{het\text{-}z1}$* (*PaSec9-1; Pa_1_11410*) was transformed into a *het-z2* background strain or when *PaSec9$^{het\text{-}z2}$* (*PaSec9-2*) was transformed into a *het-z1* background strain (Fig. S5B). Likewise, the introduction of *PaPlp1* (*plp-1* ortholog: *Pa_1_11380*) from *het-z1* strains (*PaPlp1-1*) reduced transformation efficiencies in *het-z2* strains, while the introduction of *PaPlp1-2* reduced transformation efficiencies in *het-z1* strains (Fig. S5B). As in *N. crassa*, high levels of allelic diversity were detected for *PaSec9* and *PaPlp1* in *het-z1* and *het-z2* strains (Fig. S5D; Fig. S6).

PaSec9 is also an essential gene in *P. anserina*, as homokaryotic Δ*PaSec9* strains could not be recovered. To test the role of *PaPlp1* in defining *het-z* incompatibility, *PaPlp1* was inactivated in both *het-z1* and *het-z2* backgrounds. The *ΔPaPlp1-1* and *ΔPaPlp1-2* strains retained incompatibility to *het-z2* and *het-z1* strains, respectively, but were fully compatible with each other (Fig. S5A; Table S3). *ΔPaPlp1-1* strains transformed with *PaSec9-2* acquired incompatibility to *het-z1* and *ΔPaPlp1-2* strains transformed with *PaSec9-1* acquired incompatibility to *het-z2* (Fig. S5A; Table S3). *PaSec9-2* did not lead to a

reduction in transformation efficiency when introduced into *ΔPaPlp1-1* (Fig. S5B). Collectively, these data confirmed that *PaPlp1* and *PaSec9* determine *het-z* incompatibility through non-allelic interaction between incompatible *PaPlp1* and *PaSec9* alleles (Fig. S5C). Hence, the *het-z* locus of *P. anserina* acts analogously to the *sec-9/plp-1* locus of *N. crassa*.

As shown for *N. crassa*, amino-acid differences between PaPLP1-1 and PaPLP1-2 were mainly located in the TPR region (Fig. S6B, C). Chimeric constructs in which the TPR domains were exchanged between *PaPlp1-1* and *PaPlp1-2* were introduced into *ΔPaPlp1-1* strains; the TPR domains mediated *het-z1* and *het-z2* allelic specificity (Tables S3, S4). To analyze if the patatin-like domain and the NB-ARC domain have the same essential function in PaPLP1 as in *N. crassa* PLP-1, point mutations were introduced in both domains. The two amino acids forming the catalytic dyad of the predicted patatin-like domain (S57A and D202A) and the P-loop of the NBD (K415R) of *PaPlp1-2* were mutated. Neither mutant allele reduced transformation efficiency when introduced into *het-z1* strains or conferred incompatibility to a *ΔPaPlp1-1* strain or when introduced into *ΔPaPlp1-2* strains (Fig. S5E; Table S3). These data indicated that both the phospholipase activity and nucleotide-binding domain of PaPLP1 are essential for conferring HI in *P. anserina.*

As reported above for SEC-9 of *N. crassa*, amino-acid differences between *PaSec9* allele products were mainly located in the region encoding the SNARE domains (Fig. S6A). Chimeric constructs between *PaSec9-1* and *PaSec9-2* confirmed that the SNARE domains mediate *het-z1* and *het-z2* specificity (Table S3). These data indicate that the regions of elevated variability (SNARE domain of SEC-9 and TPR domain of PLP-1) determine allelic specificity.

Convergent evolution is the most strongly supported scenario for the common use of the *plp-1*/*sec-9* system in allorecognition in three fungal genera.

The finding that three different fungal genera use the *sec-9*/*plp-1* system in allorecognition can be explained by either an independent, *de novo*, recruitment of the same genetic system for functioning in allorecognition (*i.e.* convergent evolution) or that this allorecognition genetic system was already in

use in the common ancestor of these three species, and ancient allelic lineages have been maintained by balancing selection over long evolutionary time scales (31) (*i.e*. TSP, the retention of ancient allelic lineages through speciation events). To distinguish between these two hypotheses, we aligned *sec-9* and *plp-1* sequences from the three genera *Neurospora, Podospora* and *Cryphonectria* and carried out phylogenetic inference using maximum likelihood approaches. Gene genealogies revealed that the TSP detected in *N. crassa* and *Neurospora discreta* does not extend beyond this genus. Instead, when comparing *Neurospora, Podospora* and *Cryphonectria*, different allele types of *sec-9* and *plp-1* homologs grouped by species (Fig. S6C). These data suggest that the common use of the *plp-1*/*sec-9* system in allorecognition in three divergent genera of filamentous ascomycete species is the result of convergent evolution.

Discussion

Recognition of non-self is typically dichotomized into allo- and xenorecognition, depending on whether conspecific or heterospecific (typically pathogenic) non-self is being detected (32). Allorecognition mechanisms play an important role in various aspects of multicellular life. For example, in flowering plants, self-incompatibility is a pollen recognition system that avoids inbreeding caused by self-pollination and requires co-evolution among several interacting components within the S-locus (33, 34). In basal metazoans, allorecognition responses mediate rejection between unrelated colonies, and similar to fungal HI, are controlled by highly variable genetic systems (35). Xenorecognition processes in turn are typically exemplified by responses to pathogen attack or establishment of mutualistic symbiotic interactions. Our data indicates that NLRs can be involved in both aspects of non-self recognition.

Although recent research has revealed that the repertoire of NLR-like genes in fungal genomes is quite large and variable (10), functional studies of these NLR-like genes are limited. One reason is the lack of tractable fungal pathogen systems to dissect fungal NLR-dependent immunity. However, fungal allorecognition systems, which may have evolved through exaptation similar to hybrid necrosis in plants (13), can be used to study the origin and functioning of fungal innate immunity. The fungal NLR-like protein PLP-1 induces

519 allorecognition and PCD in the three distinct filamentous fungal species, *N.*
520 *crassa, P. anserina* and *C. parasitica* (this study and (21)). PLP-1 has a tripartite
521 architecture characteristic for NLRs with a central nucleotide binding domain, an
522 N-terminal patatin-like domain and C-terminal tetratricopeptide repeats. Cell
523 death induction was dependent on both the patatin and nucleotide binding
524 domains. PLP-1 interacts with the SNARE protein SEC-9; the SNARE domains
525 were necessary and sufficient to confer allorecognition and cell death.
526 Our data supports a model whereby PCD is induced if TPR domains of
527 PLP-1 detect SNARE domains of incompatible SEC-9 proteins (Fig. 7). Upon
528 physical interaction with incompatible SEC-9 proteins, PLP-1 is activated and
529 oligomerizes into a complex that involves other proteins (shown here for PLP-2).
530 PLP-1/SEC-9 allorecognition-related cell death is dependent on the lipase
531 activity of the patatin-like domain. The finding that the N-terminal domain of
532 PLP-1 has an enzymatic activity essential for HI constitutes a novel role of NLRs,
533 as other characterized N-terminal domains of animal and plant NLRs act as
534 adaptors that perform signaling functions (36). Interestingly, patatin domains
535 have been reported to play a role in host-defense related PCD in plants (37, 38).
536 PLP-1-induced cell death could be a direct consequence of alteration of
537 membrane phospholipids via the patatin-like phospholipase domain. In this case
538 the PLP-1 complex might act as a membrane toxin itself. Alternatively, PLP-1
539 activity might rely on production of a secondary messenger and downstream
540 signaling that activates executioners of cell death. Oligomerization has been
541 shown for metazoan NLRs (15) and in plants it has recently been shown that the
542 NLR RPM1 requires self-association to be functional (39). PLP-1 also self-
543 associates and oligomerization of PLP-1 was NBD dependent. However, because
544 proteins without functional NBD (PLP-2) interact with PLP-1 during GRD, other
545 domains must contribute to protein oligomerization once PLP-1 is activated.
546 It has been proposed that the allorecognition function of fungal NLRs is
547 derived by exaptation from a function in pathogen defense (11). Based on the
548 guard-model for NLR function in plants (3), fungal NLRs would survey integrity
549 of key cellular components and trigger an immune response if pathogen effectors
550 compromise the structure of these components. The guard model for plants
551 assumes that a response is elicited when a pathogen effector disrupts a complex

552 between the guardee (a host protein) and the guard (an NLR) (12). In our model,
553 the guarding occurs indirectly, as an interaction between the compatible guardee
554 (SEC-9) and its guard (PLP-1) was not detected. Therefore, instead of disrupting
555 a complex between the guardee and the guard, in this system, a complex is
556 formed between the guard and the modified/non-self guardee, which initiates
557 downstream reactions resulting in cell death. Considering the essential role of
558 SEC-9 in exocytosis and autophagy (40), the SNARE complex might also
559 constitute a relevant cellular target for pathogen effectors. In fact, pathogenic
560 microorganisms use the SNARE motif to manipulate host membrane fusion (41).
561 For example, *Legionella* and *Chlamydia* effectors directly target membrane fusion
562 by SNARE mimicry and interactions with host SNARE proteins to create
563 intracellular compartments (42-44). In plants, the exocyst, which includes
564 SNARE proteins, was found to be targeted by effectors of fungal or oomycete
565 pathogens (45-47).
566 The level of intraspecific polymorphism in SEC-9 proteins from *N. crassa,*
567 *P. anserina* and *C. parasitica* is extreme, especially in the SNARE domains
568 essential for function. This functionally critical region of the protein also defines
569 allorecognition specificity. We hypothesize that the coiled-coil SNARE domains,
570 which are essential for vesicle fusion, have been targeted by selection in an arms
571 race with effectors aimed at inactivating exocytosis/autophagy, resulting in
572 rapid diversification of *sec-9*. The guard-model for NLR function implies that
573 protection for SEC-9 could be under surveillance of PLP-1-like NLRs. If a
574 pathogen targets or mimics the SEC-9 SNARE complex, the PLP-1 NLR is
575 activated and cell death is induced. Once established, such a two-component
576 guard/guardee system could be co-opted by exaptation into an allorecognition
577 system as genetic variants of the guardee are specifically recognized by the NLR
578 guard.
579 This report shows that the same gene pair behaves as an allorecognition
580 locus in three distantly related fungal genera (*Neurospora, Podospora,*
581 *Cryphonectria*). Other *het* genes identified in these species either showed no
582 clear orthologs or were not polymorphic. The common role for the PLP-1
583 (vic2)/SEC-9 pair in allorecognition suggests long-term conservation of the
584 derived allorecognition function. The lack of trans-species retention of ancient

allelic lineages suggests that this gene pair has been repeatedly recruited as an allorecognition system in filamentous fungi. This allorecognition system stands out among fungal recognition systems by its common role in multiple divergent species and stresses the important role of the surveillance of the essential SEC-9 SNARE in fungi. The involvement of PLP-1 in allorecognition makes this system especially tractable to study general NLR functions at the molecular level. In future studies it will be important to elucidate the exact mechanism by which PLP-1 activation induces cell death and to identify downstream contributors of the death-inducing complex. SEC-9/PLP-1 provides a powerful system for comparative analyses across biological kingdoms on the structural and molecular function of allorecognition, NLR function and downstream processes that can induce different cellular outcomes, including death.

Materials and Methods

Strain construction and growth conditions

Standard protocols for *N. crassa* can be found on the *Neurospora* homepage at the Fungal Genetics Stock Center (FGSC, http://www.fgsc.net/Neurospora/NeurosporaProtocolGuide.htm). Strains were grown on Vogel's minimal medium (VMM (48) (with supplements as required) or on Westergaard's synthetic cross medium for mating (49).

The wild *N. crassa* strains used in this study were isolated from Louisiana, USA and are available at the FGSC (17, 18, 24). FGSC 2489 served as parental strain for gene deletions and as a WT-control for all experiments, unless stated otherwise. Single deletion mutants are available at the FGSC (50, 51). Genotyping of the *Δsec-9* mutants deposited at the *Neurospora* knockout collection using *sec-9* specific primers showed that *sec-9* was still present in both mating types. When we recapitulated the knockout by homologous recombination, we were unable to purify homokaryotic hygromycin resistant ascospores from primary transformants. Therefore, *sec-9* seems to be essential in *N. crassa*. To create the *Δplp-1 Δplp-2* mutant, a deletion construct was created using the method of fusion PCR (52). Fusion PCR was also used to create constructs for swapping *sec-9*^{GRD1} with *sec-9* of different GRD specificity.

617 The plasmid pMF272 (AY598428) (53) was modified as described in (17)
618 to create *gfp*-fusions to *sec-9*, *plp-1* and *plp-2* and to express SNARE1 or SNARE2
619 of *sec-9*^{GRD3} targeted to the *his-3* locus. Site directed mutagenesis was used to
620 introduce point mutations in the NBA-ARC and the patatin-like domains of *plp-1*.
621 The plasmid pTSL88F (includes 432 bp of the terminator region of NCU00762) is
622 a derivative of the plasmid pTSL84C (54) and was used to create *mCherry*-
623 fusions to *plp-1* and *plp-2*. For expressing *plp-1* of different GRDH in the *Δplp-1*
624 *Δplp-2*; *sec-9* swap strains *plp-1.1* and *plp-1.2* including their native promoter
625 region were amplified from genomic DNA of various wild isolates (JW199,
626 JW258, JW228) and cloned into the vector pCSR1 (55) using the enzymes *Pst*I,
627 *Age*I, or *Eco*RI (5') and *Pac*I (3'). All constructs were transformed into the
628 respective *Δplp-1 Δplp-2*; *sec-9* swap strains with selection for cyclosporin
629 resistant transformants and then backcrossed for purification with the *Δplp-1*
630 *Δplp-2, his*$^{-}$ mutant.
631 Standard methods for growth and manipulation of *Podospora anserina*
632 were used as described on the *Podospora* Genome project homepage
633 (http://podospora.igmors.u-psud.fr/methods.php). Barrage assays for defining
634 incompatibility phenotypes were performed on standard DO medium. The
635 deletion cassettes were then used to transform *PaKu70::ble het-z1* or *het-z2*
636 strains (56). For cloning of the *het-z* locus six plasmids covering 57 kb of the
637 region of Pa_1_11420 (spanning from Pa_1_11380 to Pa_1_1540) were recovered
638 from a *het-z1* genomic library (generous gift of Robert Debuchy) and introduced
639 by transformation into *het-z2* strain. A single plasmid led to reduction in
640 transformation efficiency (GA0AB122CC07) and contained four genes
641 (Pa_1_11410 to 440). Deletion constructs were obtained using *Nde*I, *Sma*I, *Sph*I ,
642 *XbaI* and *Xho*I leading to deletion of one or several of the four genes. Only
643 constructs bearing Pa_1_11410 and a construct containing only Pa_1_11410 led
644 to reduction in transformation efficiency. Mutants of the catalytic site residues of
645 the Patatin domain (S57A and D202A) and P-loop (K415R) of the *PaPlp1-2*
646 product were obtained by site directed mutagenesis. The chimeric alleles of
647 *PaPlp1* with swapped TPR repeats and the chimeric alleles of *PaSec9* with
648 swapped SNARE domains were obtained by fusion PCR. Exchanged fragments
649 spanned position 1 to 660 for *PaPlp-1* and 1 to 194 for *PaSec9* (Fig. S6).

TEM analyses

Transmission electron microscopy preparations (Electron Microscopy Lab, UC Berkeley) were modified from (57). Briefly, 100 ml liquid VMM was inoculated with conidia of one or two strains at a concentration of 1×10^6 cells ml^{-1} and incubated at 30°C for 5 h (2.5h shaking at 220rpm; 2.5h standing). After harvesting by centrifugation cells were fixed with EM fix (2% glutaraldehyde, 4% paraformaldehyde, 0.04M phosphate buffer, pH 7.0) followed by 2% $KMnO_4$ treatment. Dehydration was achieved through a graded ethanol series before embedding the samples in resin.

Flow Cytometry

Cultivation for flow cytometry experiments was identical to cultivations for microscopic vacuolization assays, but agar was substituted with 20% Pluronic® F-127 (Sigma-Aldrich, USA) in VMM plates. After 4.5h – 6h cultivation at 30°C plates were put to -20°C for 10 min to liquefy the medium. Germlings were harvested by centrifugation and washed twice in cold PBS. Germlings were suspended in 1 ml PBS containing 0.1 µM SYTOX® Blue (Life Technologies, USA) and 0.15 µM propidium iodide (Sigma-Aldrich, USA) prior to analyses at a BD LSR Fortessa X20 (BD Biosciences). Two vital dyes were used as a technical control. SYTOX® Blue fluorescence was detected with a no dichroic 450/50 filter after excitation using a 405nm laser. Propidium iodide fluorescence was detected with a 685 LP 710/50 filter after excitation using a 488 nm laser. In each run 20,000 events were recorded. Each experiment was performed at least three times. Ungerminated conidia were used as a negative control in each experiment and gates were set to exclude conidia from the analysis (Fig. S1). Data were analyzed using the Cytobank Community software (community.cytobank.org). The germling death rates shown correspond to the average rate of fluorescent cells from all experiments. Because results for SYTOX® blue and propidium iodide were not significantly different (Fig. S1), results for propidium iodide are shown throughout the paper.

Microscopic vacuolization assays

Vacuolization and cell death occurred later in the strains *Δplp1Δplp2* SNARE1$^{sec\text{-}9\ GRD3}$ and *Δplp1Δplp2* SNARE2$^{sec\text{-}9\ GRD3}$. Flow cytometry could not be used to measure GRD for those strains. Instead vacuolization was quantified

683 microscopically. Conidial suspensions were prepared as described in (17). An
684 aliquot of 45 µl of conidial suspension from two strains was mixed and 80 µl of
685 this final mixture was spread on VMM agar plates (60 x 15 mm). Plates were
686 incubated for 6 ½ h -7 h at 30°C prior to vacuolization assessment. At least six
687 pictures were taken for each experiments and the percentage of vacuolized
688 germlings in the mixture was determined.
689 **Confocal microscopy**
690 Cellular localization studies were performed with a Leica SD6000
691 microscope with a 100×1.4 NA oil-immersion objective equipped with a
692 Yokogawa CSU-X1 spinning disk head and a 488 nm laser for GFP fluorescence
693 and a 563 nm laser for mCherry fluorescence controlled by the Metamorph
694 software (Molecular Devices, Sunnyvale, CA).
695 **Immunoprecipitations and Western blotting**
696 Immunoprecipitation preparations were modified from (54). 100 ml
697 liquid VMM was inoculated with conidia of one or two strains at a concentration
698 of 1×10^6 cells ml^{-1} and incubated at 30°C for 6 h (3 h shaking at 220rpm; 3 h
699 standing). Protein extraction was performed using 250µl lysis buffer as
700 described in (58) without the addition of phosphatase inhibitors.
701 Immunoprecipitation from supernatants was performed using Protein G
702 Dynabeads (Life Technologies, USA), according to the manufacturer's
703 instructions. DMP (dimethylpimelimidate) was used to covalently bind mouse
704 anti-GFP antibody (Life Technologies, USA) or rabbit anti-mCherry antibody
705 (Bio-vision, USA) to the beads.
706 **Bulked segregant analyses and genome re-sequencing**
707 Bulked segregant analysis was performed as described in (17) with minor
708 modifications. Genomic DNA was isolated from 50 progeny that underwent
709 viable fusions with FGSC 2489, but not with Segregant 2 and from 50 progeny
710 that showed GRD in fusions with FGSC 2489, but viable fusions with Segregant 2.
711 Equal amounts of DNA from 50 segregants (60 ng/segregant) were combined
712 and used for library preparations. All paired end libraries were sequenced on a
713 HiSeq2000 sequencing platform using standard Illumina operating procedures
714 (Vincent J. Coates Genomics Sequencing Laboratory, Berkeley). The mapped

reads for each group of 50 pooled segregants are available at the Sequence Read Archive (SRA) (http://www.ncbi.nlm.nih.gov/sra) (SRP121656).

Sequence analysis

The *sec-9*, *plp-1* and *plp-2* sequences of *N. crassa* and *N. discreta* wild isolates were obtained by a BLAST search (59) using NCU09243, NCU09244 and NCU09245 from FGSC 2489 as a query against *de novo* sequence assemblies from 26 wild isolates (18, 25). Introns in sequences that had no ortholog in the reference genome (i.e. *plp1.1*, *plp1.2*) were identified independently for each GRDH using AUGUSTUS (60). For phylogenetic analyses, codon alignments were carried out using MACSE (61) and visualized and processed using JALVIEW (http://www.jalview.org/). Modified multiple alignments were trimmed using TRIMAL (62). Phylogenetic trees were inferred from trimmed alignments using the default pipeline from PHYLOGENY.FR (MUSCLE, GBLOCKS, PHYML (100 bootstraps)) (63) and visualized using FIGTREE1.4 (http://tree.bio.ed.ac.uk/software/figtree/). For population genetics analyses, sequences were manually assembled and aligned, independently for each locus and each GRDH in Codoncode Aligner V. 5.1.4 (http://www.codoncode.com/aboutus.htm). Sequences were then combined by pairs of haplogroups, by pairs of paralogs or for each locus, and re-aligned using MAFFT with the E-INS-I option recommended for sequences with multiple conserved domains and long gaps (64). Summary statistics of polymorphism and divergence were computed using EGGLIB V3 (65).

Acknowledgements

This work was funded by a National Institute of General Medical Sciences grant (R01 GM060468) and by the Laboratory Directed Research and Development Program of Lawrence Berkeley National Laboratory under U.S. Department of Energy Contract No. DE-AC02-05CH11231 to NLG. JH was supported by a research fellowship from the Deutsche Forschungsgemeinschaft (HE 7254/1-1). This work used the Vincent J. Coates Genomics Sequencing Laboratory at UC Berkeley, supported by NIH S10 Instrumentation Grants S10RR029668 and S10RR027303. We thank the UC Berkeley Flow Cytometry Facility at the Cancer Research Laboratory, the Robert D. Ogg Electron Microscope Laboratory (EML)

and the Biological Imaging Facility at UC Berkeley for their technical support. We acknowledge the use of deletion strains generated by P01 GM068087 "Functional Analysis of a Model Filamentous Fungus" and which are publically available at the Fungal Genetics Stock Center. We also thank Dr. Trevor Starr for providing the plasmid pTSL88F.

Author Contributions

J.H., C.C., and N.L.G. designed research; J.H., and C.C. performed research; J.H., S.J.S., C.C. and P.G. analyzed data; and J.H., S.J.S., P.G. and N.L.G. wrote the paper.

References

1. Mekhedov SL, Makarova KS & Koonin EV (2017) The complex domain architecture of SAMD9 family proteins, predicted STAND-like NTPases, suggests new links to inflammation and apoptosis. *Biol Direct* 12(1): 13-017-0185-2.

2. Duxbury Z, *et al* (2016) Pathogen perception by NLRs in plants and animals: Parallel worlds. *Bioessays* 38(8): 769-781.

3. Jones JD, Vance RE & Dangl JL (2016) Intracellular innate immune surveillance devices in plants and animals. *Science* 354(6316): aaf6395.

4. LaRock CN & Cookson BT (2013) Burning down the house: Cellular actions during pyroptosis. *PLoS Pathog* 9(12): e1003793.

5. da Silva Correia J, Miranda Y, Leonard N, Hsu J & Ulevitch RJ (2007) Regulation of Nod1-mediated signaling pathways. *Cell Death Differ* 14(4): 830-839.

6. Urbach JM & Ausubel FM (2017) The NBS-LRR architectures of plant R-proteins and metazoan NLRs evolved in independent events. *Proc Natl Acad Sci U S A* 114(5): 1063-1068.

7. Daskalov A, Heller J, Herzog S, Fleissner A & Glass NL (2017) Molecular mechanisms regulating cell fusion and heterokaryon formation in filamentous fungi. *Microbiol Spectr* 5(2): 10.1128/microbiolspec.FUNK-0015-2016.

8. Saupe SJ (2000) Molecular genetics of heterokaryon incompatibility in filamentous ascomycetes. *Microbiol Mol Biol Rev* 64(3): 489-502.

9. Biella S, Smith ML, Aist JR, Cortesi P & Milgroom MG (2002) Programmed cell death correlates with virus transmission in a filamentous fungus. *Proc Biol Sci* 269(1506): 2269-2276.

781 10. Dyrka W*, et al* (2014) Diversity and variability of NOD-like receptors in fungi*.*
782 *Genome Biol Evol* 6(12): 3137-3158.

783 11. Paoletti M & Saupe SJ (2009) Fungal incompatibility: Evolutionary origin in
784 pathogen defense?*. Bioessays* 31(11): 1201-1210.

785 12. Jones JDG & Dangl JL (2006) The plant immune system*. Nature* 444(7117):
786 323-329.

787 13. Chae E*, et al* (2014) Species-wide genetic incompatibility analysis identifies
788 immune genes as hot spots of deleterious epistasis*. Cell* 159(6): 1341-1351.

789 14. Danot O, Marquenet E, Vidal-Ingigliardi D & Richet E (2009) Wheel of life,
790 wheel of death: A mechanistic insight into signaling by STAND proteins*.*
791 *Structure* 17(2): 172-182.

792 15. Saleh A, Srinivasula SM, Acharya S, Fishel R & Alnemri ES (1999) Cytochrome
793 c and dATP-mediated oligomerization of apaf-1 is a prerequisite for procaspase-
794 9 activation*. J Biol Chem* 274(25): 17941-17945.

795 16. DeYoung BJ & Innes RW (2006) Plant NBS-LRR proteins in pathogen sensing
796 and host defense*. Nat Immunol* 7(12): 1243-1249.

797 17. Heller J*, et al* (2016) Characterization of greenbeard genes involved in long-
798 distance kind discrimination in a microbial eukaryote*. PLoS Biol* 14(4):
799 e1002431.

800 18. Zhao J*, et al* (2015) Identification of allorecognition loci in *Neurospora crassa*
801 by genomics and evolutionary approaches*. Mol Biol Evol 32(9):2417-2432.*

802 19. Galagan JE*, et al* (2003) The genome sequence of the filamentous fungus
803 *Neurospora crassa. Nature* 422(6934): 859-868.

804 20. Williams DC & Novick PJ (2009) Analysis of SEC9 suppression reveals a
805 relationship of SNARE function to cell physiology*. PLoS One* 4(5): e5449.

806 21. Choi GH*, et al* (2012) Molecular characterization of vegetative incompatibility
807 genes that restrict hypovirus transmission in the chestnut blight fungus
808 *Cryphonectria parasitica. Genetics* 190(1): 113-127.

809 22. Arbogast BS, Edwards SV, Wakeley J, Beerli P & Slowinski JB (2002)
810 Estimating divergence times from molecular data on phylogenetic and
811 population genetic timescales*. Annu Rev Ecol Syst* 33(33): 707-740.

812 23. Corcoran P*, et al* (2014) A global multilocus analysis of the model fungus
813 *Neurospora* reveals a single recent origin of a novel genetic system*. Mol*
814 *Phylogenet Evol* 78: 136-147.

24. Ellison CE*, et al* (2011) Population genomics and local adaptation in wild isolates of a model microbial eukaryote*. Proc Natl Acad Sci U S A* 108(7): 2831-2836.

25. Gladieux P*, et al* (2015) Genomic sequencing reveals historical, demographic and selective factors associated with the diversification of the fire-associated fungus *Neurospora discreta. Mol Ecol* 24(22): 5657-5675.

26. Hall C, Welch J, Kowbel DJ & Glass NL (2010) Evolution and diversity of a fungal self/nonself recognition locus*. PLoS ONE* 5(11): e14055

27. Brennwald P*, et al* (1994) Sec9 is a SNAP-25-like component of a yeast SNARE complex that may be the effector of Sec4 function in exocytosis*. Cell* 79(2): 245-258.

28. Katz L, Hanson PI, Heuser JE & Brennwald P (1998) Genetic and morphological analyses reveal a critical interaction between the C-termini of two SNARE proteins and a parallel four helical arrangement for the exocytic SNARE complex*. EMBO J* 17(21): 6200-6209.

29. Rydel TJ*, et al* (2003) The crystal structure, mutagenesis, and activity studies reveal that patatin is a lipid acyl hydrolase with a ser-asp catalytic dyad*. Biochemistry* 42(22): 6696-6708.

30. Martinon F & Tschopp J (2005) NLRs join TLRs as innate sensors of pathogens*. Trends Immunol* 26(8): 447-454.

31. Aanen DK, Debets AJ, de Visser JA & Hoekstra RF (2008) The social evolution of somatic fusion*. Bioessays* 30(11-12): 1193-1203.

32. Rinkevich B (2004) Primitive immune systems: Are your ways my ways?*. Immunol Rev* 198: 25-35.

33. Sijacic P*, et al* (2004) Identification of the pollen determinant of S-RNase-mediated self-incompatibility*. Nature* 429(6989): 302-305.

34. Chantha SC, Herman AC, Platts AE, Vekemans X & Schoen DJ (2013) Secondary evolution of a self-incompatibility locus in the brassicaceae genus leavenworthia*. PLoS Biol* 11(5): e1001560.

35. McKitrick TR & De Tomaso AW (2010) Molecular mechanisms of allorecognition in a basal chordate*. Semin Immunol* 22(1): 34-38.

36. Bentham A, Burdett H, Anderson PA, Williams SJ & Kobe B (2017) Animal NLRs provide structural insights into plant NLR function*. Ann Bot* 119(5): 827-702.

37. Kim DS, Jeun Y & Hwang BK (2014) The pepper patatin-like phospholipase CaPLP1 functions in plant cell death and defense signaling. *Plant Mol Biol* 84(3): 329-344.

38. La Camera S, *et al* (2009) The *Arabidopsis* patatin-like protein 2 (PLP2) plays an essential role in cell death execution and differentially affects biosynthesis of oxylipins and resistance to pathogens. *Mol Plant Microbe Interact* 22(4): 469-481.

39. El Kasmi F, *et al* (2017) Signaling from the plasma-membrane localized plant immune receptor RPM1 requires self-association of the full-length protein. *Proc Natl Acad Sci U S A* 114(35): E7385-E7394.

40. Nair U, *et al* (2011) SNARE proteins are required for macroautophagy. *Cell* 146(2): 290-302.

41. Wesolowski J & Paumet F (2010) SNARE motif: A common motif used by pathogens to manipulate membrane fusion. *Virulence* 1(4): 319-324.

42. Shi X, Halder P, Yavuz H, Jahn R & Shuman HA (2016) Direct targeting of membrane fusion by SNARE mimicry: Convergent evolution of *Legionella* effectors. *Proc Natl Acad Sci U S A* 113(31): 8807-8812.

43. Delevoye C, *et al* (2008) SNARE protein mimicry by an intracellular bacterium. *PLoS Pathog* 4(3): e1000022.

44. Arasaki K, *et al* (2017) *Legionella* effector Lpg1137 shuts down ER-mitochondria communication through cleavage of syntaxin 17. *Nat Commun* 8(8): 15406.

45. Du Y, Mpina MH, Birch PR, Bouwmeester K & Govers F (2015) *Phytophthora infestans* RXLR effector AVR1 interacts with exocyst component Sec5 to manipulate plant immunity. *Plant Physiol* 169(3): 1975-1990.

46. Yun HS, Kang BG & Kwon C (2016) *Arabidopsis* immune secretory pathways to powdery mildew fungi. *Plant Signal Behav* 11(10): e1226456.

47. Fujisaki K, *et al* (2015) Rice Exo70 interacts with a fungal effector, AVR-pii, and is required for AVR-pii-triggered immunity. *Plant J* 83(5): 875-887.

48. Vogel HJ (1956) A convenient growth medium for *Neurospora*. *Microbial Genetics Bulletin* 13: 42-46.

49. Westergaard M & Mitchell HK (1947) *Neurospora* V. A synthetic medium favoring sexual reproduction. *Amer J Bot* 34: 573-577.

50. Colot HV, *et al* (2006) A high-throughput gene knockout procedure for *Neurospora* reveals functions for multiple transcription factors. *Proc Natl Acad Sci U S A* 103(27): 10352-10357.

885 51. Dunlap JC*, et al* (2007) Enabling a community to dissect an organism:
886 Overview of the *Neurospora* functional genomics project*. Adv Genet* 57: 49-96.

887 52. Szewczyk E*, et al* (2006) Fusion PCR and gene targeting in *Aspergillus*
888 *nidulans. Nat Protoc* 1(6): 3111-3120.

889 53. Freitag M, Hickey PC, Raju NB, Selker EU & Read ND (2004) GFP as a tool to
890 analyze the organization, dynamics and function of nuclei and microtubules in
891 *Neurospora crassa. Fungal Genetics and Biology* 41(10): 897-910.

892 54. Jonkers W*, et al* (2014) HAM-5 functions as a MAP kinase scaffold during cell
893 fusion in *Neurospora crassa. PLoS Genet* 10(11): e1004783.

894 55. Bardiya N & Shiu PK (2007) Cyclosporin A-resistance based gene placement
895 system for *Neurospora crassa. Fungal Genet Biol* 44(5): 307-314.

896 56. El-Khoury R*, et al* (2008) Gene deletion and allelic replacement in the
897 filamentous fungus *Podospora anserina. Curr Genet* 53(4): 249-258.

898 57. Fleissner A, Diamond S & Glass NL (2009) The *Saccharomyces cerevisiae*
899 PRM1 homolog in *Neurospora crassa* is involved in vegetative and sexual cell
900 fusion events but also has postfertilization functions*. Genetics* 181(2): 497-510.

901 58. Pandey A, Roca MG, Read ND & Glass NL (2004) Role of a mitogen-activated
902 protein kinase pathway during conidial germination and hyphal fusion in
903 *Neurospora crassa. Eukaryot Cell* 3(2): 348-358.

904 59. Altschul SF, Gish W, Miller W, Myers EW & Lipman DJ (1990) Basic local
905 alignment search tool*. J Mol Biol* 215(3): 403-410.

906 60. Stanke M & Morgenstern B (2005) AUGUSTUS: A web server for gene
907 prediction in eukaryotes that allows user-defined constraints*. Nucleic Acids Res*
908 33(Web Server issue): W465-7.

909 61. Ranwez V, Harispe S, Delsuc F & Douzery EJ (2011) MACSE: Multiple
910 alignment of coding SEquences accounting for frameshifts and stop codons*. PLoS*
911 *One* 6(9): e22594.

912 62. Capella-Gutierrez S, Silla-Martinez JM & Gabaldon T (2009) trimAl: A tool for
913 automated alignment trimming in large-scale phylogenetic analyses*.*
914 *Bioinformatics* 25(15): 1972-1973.

915 63. Dereeper A*, et al* (2008) Phylogeny.fr: Robust phylogenetic analysis for the
916 non-specialist*. Nucleic Acids Res* 36(Web Server issue): W465-9.

917 64. Katoh K & Standley DM (2013) MAFFT multiple sequence alignment software
918 version 7: Improvements in performance and usability*. Mol Biol Evol* 30(4): 772-
919 780.

65. De Mita S & Siol M (2012) EggLib: Processing, analysis and simulation tools for population genetics and genomics. *BMC Genet* 13: 27-2156-13-27.

Figure Legends

Fig. 1: Germling regulated death is induced if genetically incompatible germlings undergo cell fusion. A: When GRD1 germlings (FGSC 2489) marked with cytoplasmic GFP (green, top right) undergo cell fusion with FM4-64 stained GRD1 germlings of Segregant 18 (red, bottom left) no death occurred as indicated by the absence of SYTOX® Blue fluorescence (bottom right). Note that fusion has occurred because GFP has entered Segregant 18. **B:** When GRD1 germlings (FGSC 2489) marked with cytoplasmic GFP (green, top right) fused with FM4-64 stained GRD2 germlings of Segregant 2 (red), vacuolization and death occurred as indicated by strong SYTOX® Blue fluorescence (bottom right). **C-D:** Transmission electron micrograph of GRD1 germlings (FGSC 2489) undergoing self fusion **(C)** or Segregant 2 germlings undergoing self fusion **(D)** showed healthy cells with no signs of death. **E:** In a mixture of GRD 1 germlings (FGSC 2489) and GRD3 germlings (Segregant 2), fused cells showed vacuolization, plasma membrane detachment from the cell wall, and organelle degradation. Arrows indicate fusion points. Scale bars: 10 μm.

Fig. 2: *sec-9, plp-1* and *plp-2* within the Germling Regulated Death Haplotype (GRDH) region show trans-species polymorphism. **A:** Genomic organization of germling regulated death haplotype (GRDH) regions in *Neurospora crassa* wild isolates. Genomic rearrangements within the GRDH spanned the genetic interval between NCU09237 and NCU09253 (shown are the last two digits of NCU numbers) and included duplications of NCU09244, a deletion of NCU09245 and inversions. Alleles at NCU09243 (*sec-9*) and NCU09244 (*plp-1*) within a GRDH show high DNA sequence identity, but are diverse between GRDHs. The percent DNA identity between alleles in members of the different GRDH groups of selected genes across the genetic interval in comparison to FGSC 2489 (a member of GRDH1) are shown. **B**: Coding sequences from 23 *N. crassa* wild Louisiana isolates and eight *N. discreta* wild isolates were used to build maximum likelihood phylogenetic trees for NCU09242 and

NCU09243 (*sec-9*) using the default pipeline from PHYLOGENY.FR (63). Bootstrap values are given for each node. Black bars indicate substitution rates. GRDH1 isolates are shown in yellow, GRDH2 isolates are shown in green, GRDH3 isolates are shown in blue, and GRDH4 isolates are shown in purple. *N. discreta* isolates are shown in red. Note nesting of *N. discreta* isolates within *N. crassa* lineages for NCU09243 (*sec-9*) but not for NCU09242. See Figure S2D, E for phylogenetic trees of NCU09244/NCU09245, NCU16494, and NCU09247. **C:** SEC-9-GFP (left) localizes to the cytoplasm and concentrates at a crescent at the tips of germ tubes (arrowheads). Cytosolic localization might reflect cleaved GFP as apparent from Western blot analyses (see Fig. 6). PLP-1-GFP and PLP-1-mCherry (middle) predominantly localize to the periphery of the cell. PLP-2-GFP and PLP-2-mCherry (right) also predominantly localize to the periphery of the cell; localization to the vacuoles is common in mCherry-tagged proteins in *N. crassa*. Scale bars: 10 μm.

Fig. 3: Genetic interaction of *sec-9* and *plp-1* mediate GRD. A: Germling death frequencies of *Δplp-1, Δplp-2* and *Δplp-1 Δplp-2* cells after fusion with their GRD1 (FGSC 2489) parental strain or with a GRD3 (Segregant 2) strain. Germling death rates were determined using flow cytometry. Experiments were performed at least in triplicates with 20,000 events counted per experiment. Student's *t* test, ***: $p < 0.001$ **B:** Strategy for creating *Δplp-1 Δplp-2* and *Δplp-1 Δplp-2, sec-9*^{swap} strains by homologous recombination. **C:** Germling death frequencies of *Δplp-1 Δplp-2, sec-9*^{swap} strains (colors correspond to GRDH of the *sec-9* swap) with FGSC 2489, *Δplp-1, Δplp-2* and *Δplp-1 Δplp-2* strains (all GRD1 background). Germling death frequencies were determined using flow cytometry. Experiments were performed at least in triplicates with 20,000 events counted per experiment. Student's *t* test, **: $p < 0.01$, ***: $p < 0.001$.

Fig. 4: Polymorphic SNARE motifs of SEC-9 are recognized by PLP-1 during GRD. A: Schematic presentation of SEC-9 of *N. crassa*. SEC-9 has an N-terminal extension and two C-terminal SNARE-motifs. **B:** Consensus sequence conservation of SEC-9 within 23 wild isolates of a *N. crassa* population along every amino acid position. Note the higher conservation within the N-terminal

region. **C:** Germling death frequencies of *Δplp-1 Δplp-2, sec-9^{chimera1}* (left two columns; chimera pictured below) and *Δplp-1 Δplp-2, sec-9^{chimera2}* (right two columns; chimera pictured below) in pairings with GRD1 (FGSC 2489) or GRD 3 (Segregant 2) germlings. Colors correspond to the respective GRDH (yellow = GRDH1; blue = GRDH3). Death rates were measured by flow cytometry. Experiments were performed at least in triplicates with 20,000 events counted per experiment. Student's *t* test, **: $p < 0.01$, ***: $p < 0.001$. **D:** Vacuolization frequency of *Δplp-1 Δplp-2,* SNARE1^{GRD3} or *Δplp-1 Δplp-2,* SNARE2^{GRD3} germlings undergoing self-fusion (columns 2, 4), or when paired with GRD1 germlings (FGSC 2489). *Δplp-1 Δplp-2, sec-9^{GRD3}* served as a positive control. Vacuolization rates were determined by microscopy. Experiments were performed in triplicates with at least 350 germlings evaluated per experiment. Student's *t* test ***: $p < 0.001$. **E**: Alignment of the SN1 and SN2 SNARE regions of the SEC-9 homologs from *N. crassa* wild isolates (N.c)*, Podospora anserina* (P.a)*, Cryphonectria parasitica* (C.a) with SNARE domains of yeast SEC9 (S. c.) and human SNAP25 (H.s), using ClustalOmega. For the *N. crassa, P. anserina* and *C. parasitica* sequences, for each site, the average of all intraspecific pairwise alignment scores (extracted from Jalview) were calculated and then normalized to set the most divergent site to 100 (red) and the most conserved site (no intraspecific polymorphism) to 0 (blue). For *N. crassa* in SN2, only three of the four allelic types were used, as the JW22 sequence could not unambiguously be aligned without gaps. Black dots indicate interfaces with SS0-1/SNC-2, empty dots indicate self-interface (SEC-9 SNARE1 with SNARE2).

Fig. 5: The patatin-like domain and nucleotide binding domain of PLP-1 are essential for GRD. A: Schematic presentation of PLP-1. PLP-1 has a tripartite domain architectures with an N-terminal domain (patatin-like), a central nucleotide-binding domain (NBD) and C-terminal tetratricopeptide repeats (TPR). **B:** Alignment of patatin phospholipase domains of PLP-1^{GRD1} and PLP-1^{GRD3} of *N. crassa* (N.c), PaPLP1-1 of *P. anserina* (P.a), patatin from potato (S.t), and human iPLA2 (H.s). The GGxR/K motif (*) and the catalytic dyad formed by a serine and aspartic acid (▼) are conserved. Essential amino acids that have been mutated to alanine in PLP-1 are encircled. **C:** Alignment of NBD domains of PLP-

1019 1^{GRD1} and PLP-1^{GRD3} of *N. crassa* (N.c), PaPLP1-1 of *P. anserina* (P.a), DRL24 of
1020 *Arabidopsis thaliana* (A.t), tomato K4BY49 (S.l), and human APAF1 (H.s). The
1021 Walker A motif (*), the Walker B motif (+) and the nucleotide sensor 1 (^)
1022 residues are conserved. Essential amino acids that have been mutated to alanine
1023 in PLP-1 are encircled. **D:** Localization of PLP-1 is not affected by mutations
1024 introduced in the patatin-like domain (S63A, D204A: green) or in the NB-ARC
1025 domain (K414A, D484A: purple). Scale bars: 10 µm **E:** Germling death
1026 frequencies are reduced when GRD1 strains expressing PLP-1 with mutations in
1027 the patatin-like domain and in the NB-ARC domain are paired with a strain
1028 expressing SEC-9^{GRD3}. Colors correspond to the domain affected by the mutations
1029 (red = control strains, green = patatin-like, purple = NB-ARC). Germling death
1030 frequencies were determined using flow cytometry. Experiments were
1031 performed at least in triplicates with 20,000 events counted per experiment.
1032 One-way ANOVA with post-hoc Tukey HSD Test $p<0.05$.
1033
1034 **Fig. 6: Interaction studies by co-immunoprecipitation experiments.** Input
1035 panels show Western blots of total protein extracts isolated from 6 hr-old
1036 germlings probed with either anti-GFP antibodies (A, B) or anti-mCherry
1037 antibodies (C, D). IP panels show anti-mCherry (A, B) or anti-GFP (C, D)
1038 immunoprecipitated proteins probed with anti-mCherry (A, B) or anti-GFP
1039 antibodies (C, D). Co-IP panels show anti-mCherry (A, B) or anti-GFP (C, D)
1040 immunoprecipitated proteins probed with anti-GFP (A, B) or anti-mCherry (C, D)
1041 antibodies. Parentheses indicate tagged proteins that are expressed in one
1042 heterokaryotic strain. **A:** Heterokaryotic germlings expressing various
1043 combinations of tagged GRD1 proteins were cultivated. GRD was triggered by co-
1044 cultivation of a heterokaryotic strain (PLP-1-GFP / PLP-1-mCh) with a GRD3
1045 strain (lane 2). **B:** Heterokaryotic germlings expressing various combinations of
1046 tagged GRD1 proteins were co-cultivated with germlings of GRD3 specificity to
1047 induce GRD. **C:** Germlings expressing tagged proteins as indicated were co-
1048 cultivated to induce germling fusion between the strains. During cultivation, GRD
1049 occurred if wild type PLP-1 interacted with SEC-9^{GRD3} (lane 2, 4, 5). Tagged SEC-9
1050 was expressed in addition to endogenous SEC-9^{GRD1} and was either
1051 overexpressed by the *tef-1* promoter (OE) or controlled by the native *sec-9*

promoter (lane 5, 6, 7). Note that there is a size difference between SEC-9^{GRD1} (43.5kDa) and SEC-9^{GRD3} (47 kDa). **D:** Heterokaryotic germlings expressing various combinations of tagged GRD1 proteins were co-cultivated with germlings of a *Δplp-1 Δplp-2, sec-9^{GRD3}* strain. During cultivation, GRD occurred if wild type PLP-1 interacted with SEC-9^{GRD3} (lanes 1, 2, 3) while in combinations with mutated PLP-1 no GRD occurred (S64A, D204A, K414A) or GRD was reduced (D484A) (compare Fig. 5E). PLP-1-GFP: ~175 kDa, PLP-2-GFP: ~90 kDa, SEC-9-GFP: ~70 kDa, GFP: ~25 kDa, mCherry: ~30 kDa. For reciprocal co-immunoprecipitations see Figure S4.

Fig.7: Model for NLR function of PLP-1. Our data suggest that PLP-1 functions as a fungal NOD-like receptor that seems to act in a similar way to plant and animal NLRs. Our model states that PLP-1 is kept in an inactive conformation when not induced. Interaction with SEC-9 of different GRD specificity activates PLP-1. Recognition is predicted to occur via the TPR domain and the SEC-9 SNARE domains, as these regions confer allelic specificity. The involvement of other proteins cannot be excluded. Activation of PLP-1 induces oligomerization of PLP-1, which requires a functional NB-ARC domain. Once initiated, proteins without functional NB-ARC domain can participate in the GRD complex (PLP-2). The GRD signal for cell death is transmitted via the N-terminal patatin-like phospholipase activity.

Figures

Figure 1

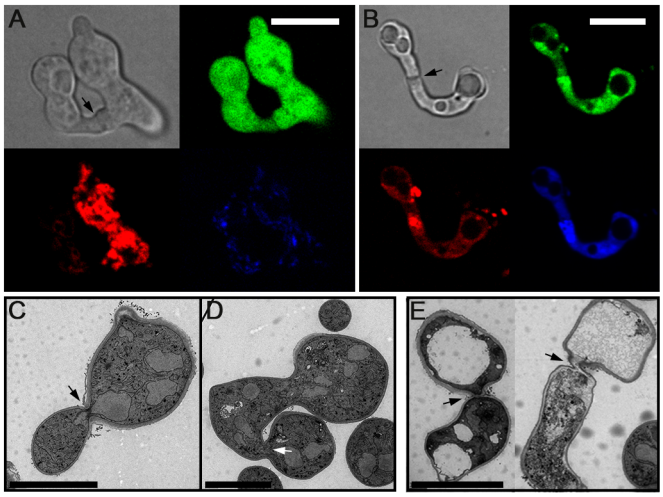

Figure 2

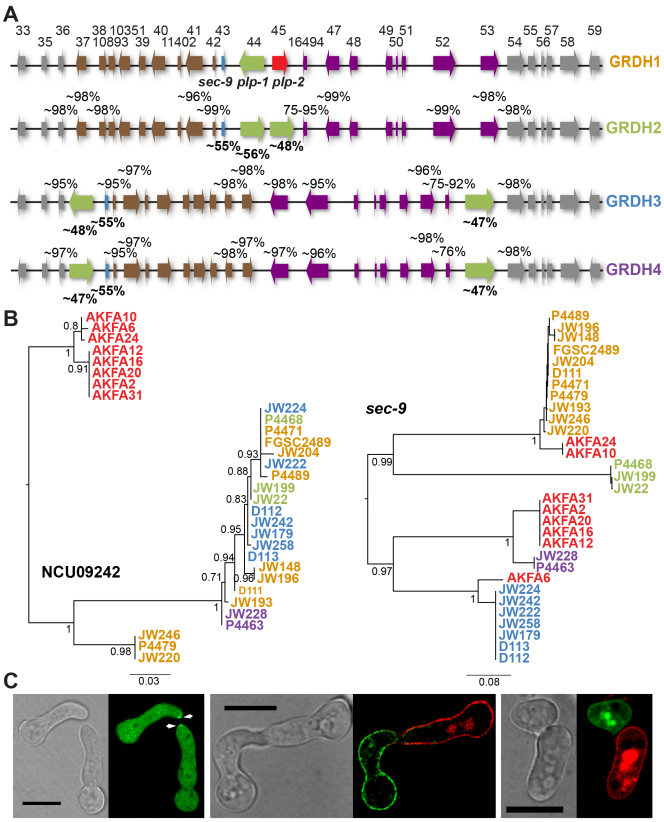

Figure 3

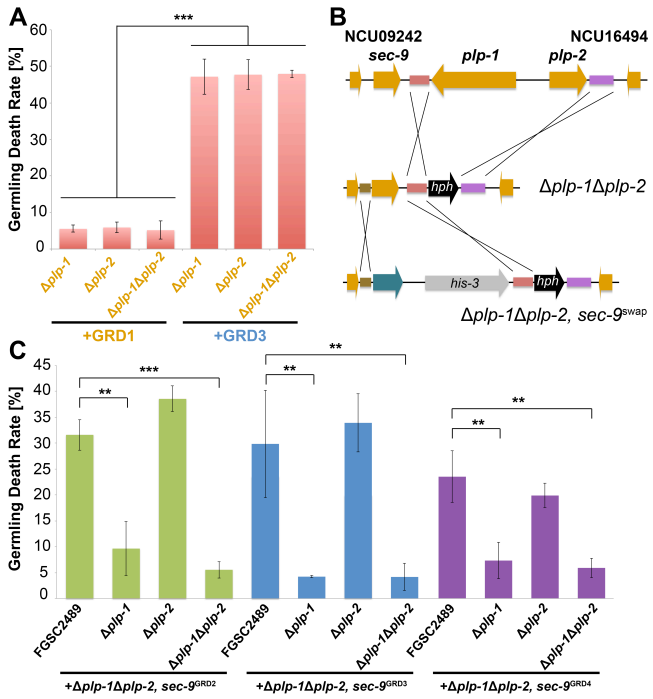
A
Germling Death Rate [%]
***
Δplp-1
Δplp-2
Δplp-1Δplp-2
Δplp-1
Δplp-2
Δplp-1Δplp-2
+GRD1
+GRD3
B
NCU09242
sec-9
plp-1
plp-2
NCU16494
hph
Δplp-1Δplp-2
his-3
hph
Δplp-1Δplp-2, sec-9swap
C
Germling Death Rate [%]
FGSC2489
Δplp-1
Δplp-2
Δplp-1Δplp-2
+Δplp-1Δplp-2, sec-9GRD2
+Δplp-1Δplp-2, sec-9GRD3
+Δplp-1Δplp-2, sec-9GRD4

Figure 4

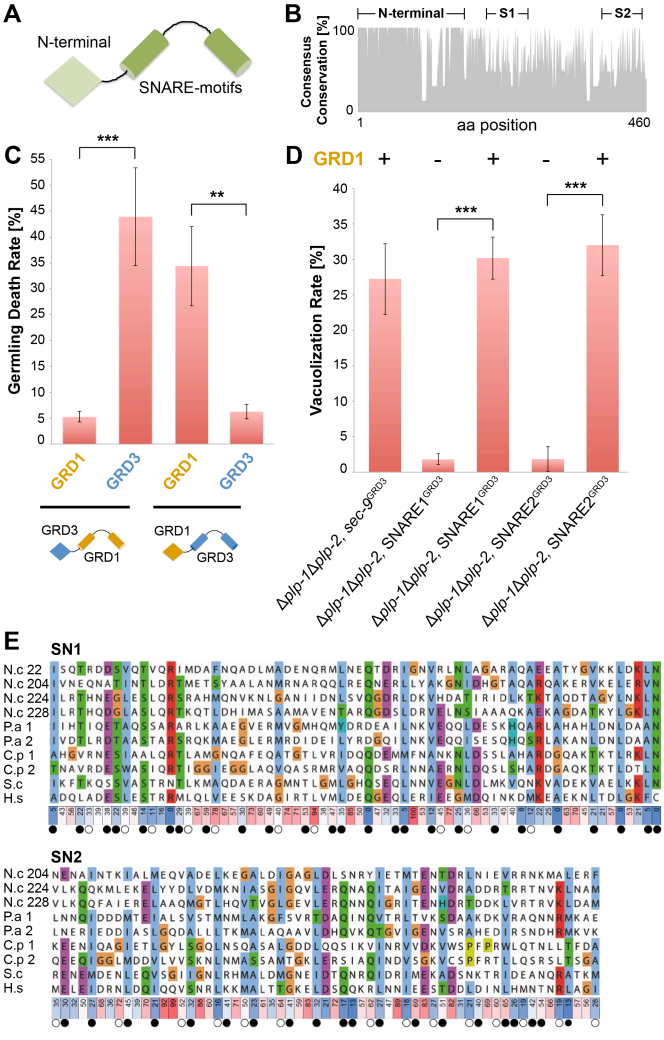

Figure 5

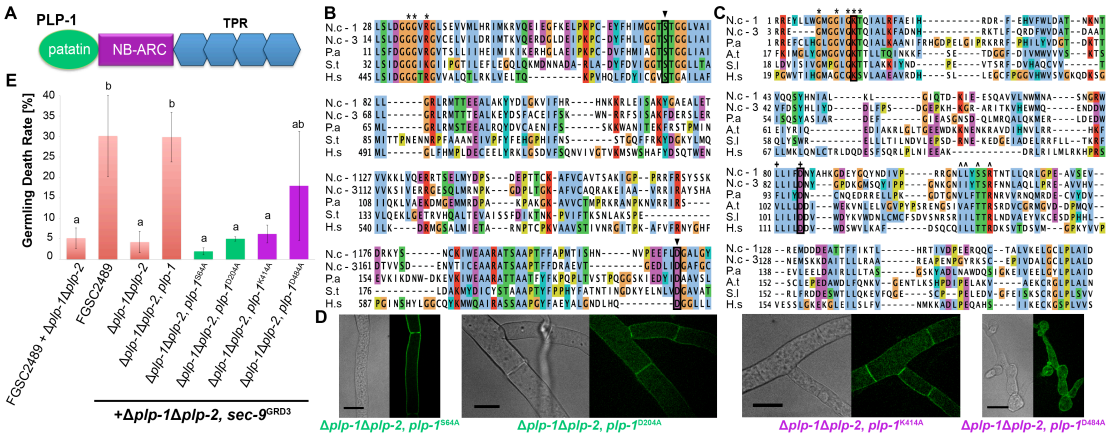

Figure 6

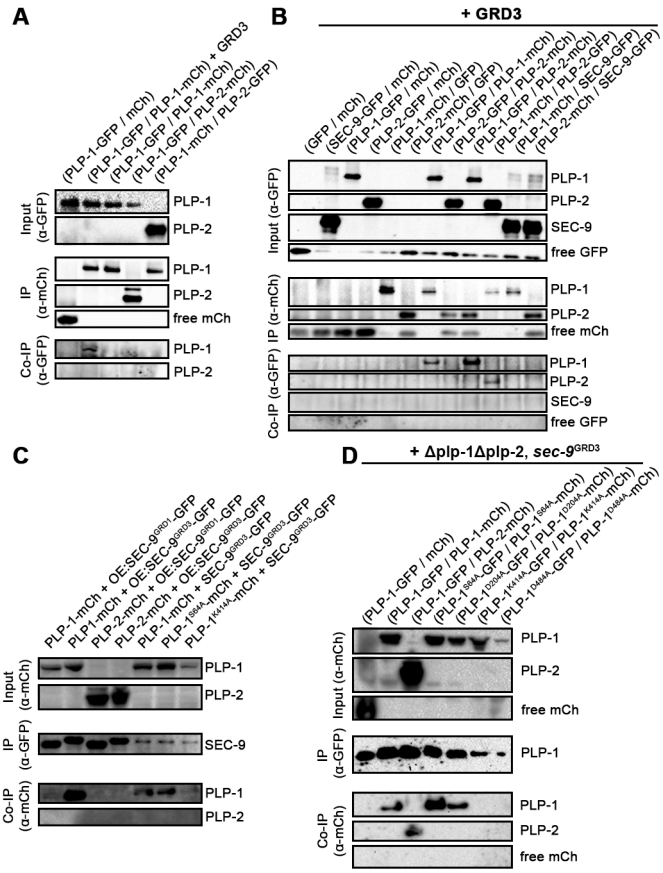

Figure 7